Journal of Materials and Electronic Devices 1 (2022) 28-35

Shape Memory Alloy Layered CuAlFeMn/n-Si/Al Photodiode with a High Photo-responsivity Merit and Negative Capacitance

Oktay Karaduman[1], Canan Aksu Canbay[1]*

[1]Department of Physics, Science Faculty, Firat University, Elazig, 23119, TURKEY

In this study, a new Schottky MS contact type CuAlFeMn/n-Si/Al photodiode was fabricated via coating thin film CuAlFeMn shape memory alloy with a different composition on n-type silicon substrate by using thermal evaporation method. The photoelectrical diode/photodiode characterization of the produced photodevice was conducted by taking photo-electrical current-voltage (I-V), dynamic current-time (TPC, I-t) and capacitance-voltage (C-V) measurements in dark condition and under different artificial day light conditions. The obtained characteristic forward bias I-V plots revealed the photovoltaic and photoconductive properties. Excellent responsivity and good detectivity maxima values were achieved. The photovoltaic behavior of the produced photodiode was apparently observed on the TPC light-on/light-off patterns. Negative capacitance occurrence was observed by taking the capacitance-voltage measurements.

Keywords: *Schottky Photodiodes, Thin film shape memory alloys, Martensite, Responsivity, Space charge limited current, Detectivity, Negative capacitance*

Submission Date: 19 February 2022
Acceptance Date: 04 May 2022

**Corresponding author: caksu@firat.edu.tr*

1. Introduction

Metal-semiconductor (MS) contact diodes with an interface potential barrier called as Schottky barrier height (SBH) can separate photoexcited electron-hole pairs [1]. This enabled the production of MS Schottky barrier type photodiodes, other photodetectors and sensors, transistors, solar cells or other photodevices in nanotechnology mostly based on silicon [1–14].

Generally, thin films of single metal elements (like Au, Pt, Cu, Ag etc.) are used to form top Schottky contacts in fabrication of MS Schottky photodevices based on the work functions of those metal elements. Work functions and thermal and electrical conductivity values of metal alloys can tunably differ than those constant values of single metal elements. Therefore, using thin film alloys in Schottky contacts increases the number of different choices. The use of thin film NiTi shape memory alloys (SMAs) in fabrication of Schottky diodes have been tried on in 1990s [15–17], too. But thin film SMAs have firstly been used in production of Schottky MS photodiodes just after a few years ago [18–24]. In these works Cu-based SMAs were used as thin film contacts, since Cu-based SMAs have larger electrical and thermal conductivities and much cheaper than NiTi SMAs.

SMAs are a famous smart material group due to that they can show some highly desirable and fascinating useful properties like shape memory effect (SME) and superelasticity (SE). Therefore these alloys are preffered to utilize as in bulk, micro or nano sizes in many technological and industrial areas such as actuator, medical, robotic, automotive, aerospace, micro or nano electromechanical systems (N/MEMs) etc. [25–37]. The

shape recocery or shape memory effect mechanism of these materals depends on an atomically diffusionless, isothermal and reversible solid to solid phase transitions (named as martensitic transformations) induced fundamentally by heat [25]. Such transformations occur between cold martensite (M) and hot austenite (A) solid phases in a SMA. The transformation induced by temperature change can be provided by many kind of external stimuli such as heat, mechanical stres, electric or magnetic field or optic radiation. By a transformation from martensite to austenite phase, the shape of a deformed SMA in martensite structure changes to its original predeformed shape as a sum of microcrystallographic phase changes triggered by internal stresses induced by heat.

In the mentioned recent works [18–24] done on the fabrication of thin film SMA layered Schottky photodiodes, good diode characteristics and photoconductive, photovoltaic properties have been achieved. But these works still are of a few number. More research can be done to investigate and improve such SMA/semiconductor contact devices. Some of the ways for doing this can be using different type SMAs and/or with different compositions, deploying an organic or metal-oxide insulator interlayer, producing with varied semiconductor substrates or by different production methods.

In this work, a new MS Schottky barrier photodiode was by island-like deposition of thin film CuAlFeMn SMA on n-Si substrate via thermal evaporation technique. The diode parameters, photodiode figure of merits and capacitance of the produced photodevice were characterized by taking photo-electrical I-V, I-t tests under dark and varied light conditions and stepped-frequency based C-V measurements.

2. Materials and Experimental Method

The CuAlFeMn SMA with a composition of 73.23Cu-21.93Al-3.36Fe1.48Mn (at.%) that used in this work as thin film Schottky metal contact was previously fabricated by arc melting and the shape memory effect characterization tests were done on this alloy, all of the experimental details about this CuAlFeMn SMA were given in the previous works [38,39], but thermal and structural DSC and XRD characterization tests results of this SMA showing its shape memory effect properties are to be given briefly in the results section of this work, too. For fabrication of the CuAlFeMn/n-Si/Al photodiode at first the n-Si wafer and pieces of CuAlFeMn SMA and Al were cleaned by RCA standard cleaning procedure that includes ultrasonic washing bath in distilled water, acetone and ethyl alcohol for 5 min each, etching the n-Si wafer in (1:10 ml) HF:H2O acid medium for 30 s, then again washing by distilled water and at last drying with nitrogen gas. After cleaning, at first Al metal film with 150 nm thickness was coated on back face of n-Si to form ohmic contact by using a Nanovak thermal evaporation system as the chamber of evaporator reached to 2×10^{-6} Pa of pressure. Then the obtained n-Si/Al structure was annealed at 570 °C for 5 min for diffusion of n-Si and Al surfaces to each other and thus getting better contact quality. Then, CuAlFeMn SMA thin film with 150 nm thickness was similarly deposited as island-like spots on the mask shadowed front face of the n-Si/Al ohmic structure and thus the fabrication CuAlFeMn/n-Si/Al photodiode was completed. Each hole of the used mask has an area (A) of 0.785×10^{-2} cm^2 that is also the diode area of each top island-like CuAlFeMn SMA film contacts. The current-voltage (I-V), capacitance-voltage (C-V) and current-time (I-t) diode/photodiode characterization tests were made under dark and different light power intensities by using FYM-7000 and -9000 model FYTRONIX Solar Simulator electronic characterization systems. A diagramatic view of the fabricated shape memory alloy thin film based photodiode is presented in Figure 1.

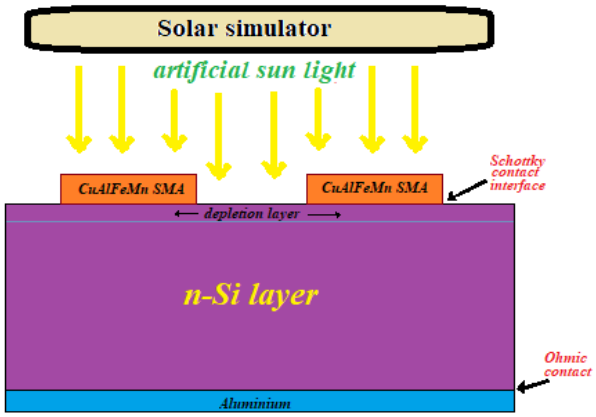

Fig.1. A diagramatic view of the fabricated CuAlFeMn/n-Si/Al photodiode.

.

3. Results and Discussions

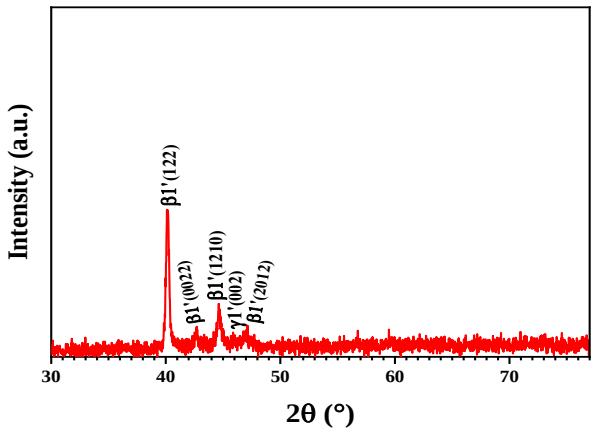

Fig.2. The microstructural X-ray diffraction pattern of the CuAlFeMn shape memory alloy.

The XRD (X-ray diffraction) graphic of the CuAlFeMn SMA (obtained by using CuKα type X-rays) is given in Figure 2. As seen on this diffraction pattern, the highest peak of β1'(122) is the dominant martensite phase formed in this alloy, and the shorter β1'and γ1' peaks ar the other appeared peaks [38,39]. These martensite peaks found in the CuAlFeMn alloy confirms that the microstructural shape memory behavior mechanism do exist in this alloy.

The DSC (differential scanning calorimetry) thermogram curves of the CuAlFeMn shape memory alloy obtained at different heating/cooling rates between 5-45 °C/min are presented in Figure 3. The reversible endothermic and exothermic martensitic transformation peaks that were appeared on each one of these curves indicate the M→A (on heating the alloy) and then A→M (on cooling the alloy), respectively [40–43]. Therfore it can be said that the CuAlFeMn alloy has a shape memory effect property which is a result of thermal response of this alloy against the increasing/decreasing temperature changes occurred in the alloy by the each heating/cooling DSC run cycle. By analyzing these peaks via applying tangent method of DSC software on them, the determined some thermodynamical martensitic transformation temperatures (A_s, A_f, M_s and M_f), hysteresis gap (A_s-M_f), max-peak temperature (A_{max}) of M→A transition, equilibrium temperature (T_0), and the enthalpy (ΔH) and entropy (ΔS) change values of M→A transformation all for the curve obtained at the heating/cooling rate of 25 °C/min are given in Table 1.

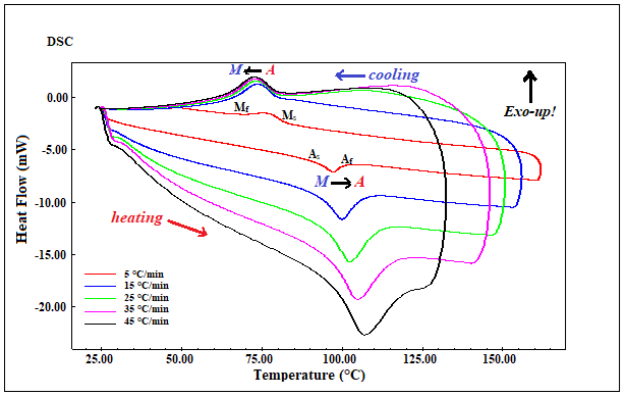

Fig.3. The DSC cycling curves showing the reversible martensitic M↔A phase transitions as a thermal response of the CuAlFeMn shape memory alloy.

Table-1: The thermo-responsive characteristic martensitic phase transition temperatures and the other transformational parameters values for the CuAlFeMn shape memory alloy.

DSC heating/cooling rate (°C/min)	A_s (°C)	A_f (°C)	A_{max} (°C)	M_s (°C)	M_f (°C)	A_s-M_f (°C)	T_0 (°C)	$\Delta H_{M\rightarrow A}$ (J/g)	$\Delta S_{M\rightarrow A}$ (J/g°C)
25	93.56	111.44	102.52	79.90	64.70	31.54	95.67	7.09	0.074

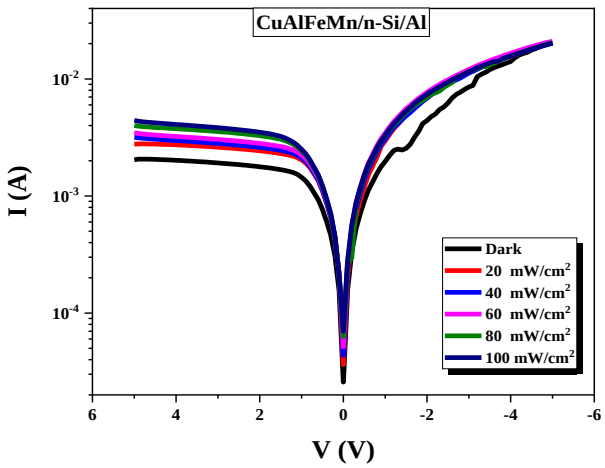

Fig.4. The multiple semi-log *ln(I)-V* plots of the CuAlFeMn/n-Si/Al photodiode obtained under dark and varied steps of light power intensity conditions.

The results obtained from the photo-electrical I-V tests as multiple semi-log *ln(I)-V* plots for the novel CuAlFeMn/n-Si/Al SMA-photodiode under dark and step-increased light power intensities are presented in Figure 4. On these plots, the current was allowed to conduct by the photodiode only in the positive forward voltage bias on the right side (in the figure negative voltage is seen on the right side due to the opposite signed test probe use), except a smaller saturation (leakage) current (I_0) was allowed to conduct in the reverse voltage bias region (on the left side). Thus, the photodiode shows a current rectifying characteristic. However, although the magnitudes of the photocurrents seen in the reverse (left side) voltage region are remarkably high, the magnitute of the dark leakage current is found abnormally high most probably caused from the remained contamination, interface states, vacancies and impurities in the CuAlFeMn/n-Si interface. Therefore, by using RR(±V) = I(V)/I(-V) formula [22], the values of the current rectification ratio (RR) parameter of the photodiode (at ±5 V of voltage couple equal-in-absoulte) were determined as 10.04 for dark and 4.58 for 100 mW/cm^2 of light power intensity conditions, respectively [22], which are found very low due to the high leakage current. The RR should be increased by making better wafer surface cleaning. Nevertheless, the levels of the photocurrents generated by the applied light [22] are

enormously high. The generation of photocurrents (seen as the bounced current levels in the left reverse voltage region by the effect of increasing light power) means that the electromagnetic light radiation changes the electrical conductivity of the photodiode which is defined as the photoconductivity property of this produced photodevice. These photocurrents (or electron-hole pairs) generated photoelectrically by the absorbed incident light photons with sufficient energies larger than the band gap (E_g) of n-Si ($h\nu \geq E_g$) stimuling the electrons in the valance band. For a Schottky MS diode (or photodiode) the relationship between current and voltage depending on the conventional Schottky emission, also known as the thermionic emission (TE) theory, is expressed by the formula [1,22] (for V>3kT/q condition) given as below;

$$I = I_o exp\left(\frac{q(V-IR_S)}{nkT} - 1\right). \quad ..(1)$$

where; *V-IRs* stands for the voltage that drops across the metal-semiconductor junction, *k* is the Boltzmann constant, *q* is electron charge, *T* is temperature (T= 300 K), *n* is idealty factor (unitless) parameter of the diode, and I_0 is the reverse saturation current. By intercepting the linear fragment of *ln(I)-V* plot positioned in forward bias region, the I_0 value can be found by the formula given as below;

$$I_0 = AA^*T^2 exp\left(-\frac{q\phi_b}{kT}\right) \quad (2)$$

where; *A** is Richardson constant (its theoretical value for n-Si is 112 $A.cm^{-2}K^{-2}$) [1,5], ϕ_b refers to the Schottky barrier height (SBH) of the produced CuAlFeMn/n-Si/Al photodiode at zero voltage (V=0), and *A* is the diode's area of the CuAlFeMn top metal contact ($A=0.785\times10^{-2}$ cm^2).The ideality factor *n* values were calculated by substituting the slope values found by taking linear fittings on the line fragments of the *ln(I)-V* plots at forward bias in the formula presented as below;

$$n = \frac{q}{kT}\left(\frac{dV}{d(ln\, I)}\right) \quad (3)$$

Thus, the values of the *n* ideality factor parameter of the CuAlFeMn/n-Si/Al photodiode were computed as 14.8 for dark condition and 13.7 for the light condition with 100 mW/cm^2 of power intensity. These *n* values were found higher than the ideal value (*n*=1). The reasons for the *n* values deviated from the unity (n > 1) were explained by the effects of impurities and vacancies, interface states (traps), non-uniform charge distribution in the interface and the non-homogenous ϕ_b barrier height (SBH) across the MS contact [1,5,8,22]. The ϕ_b values of the the produced photodiode can be determined by using the formula [22] given as below;

$$\phi_b = \frac{kT}{q} ln\left(\frac{AA^*T^2}{I_0}\right) \quad .(4)$$

The ϕ_b value of the SMA layered CuAlFeMn/n-Si/Al photodiode was calculated as 0.491 eV for dark condition and 0.482 eV for 100 mW/cm^2 of light intensity condition.

One of the important photodiode figure of merits is the responsivity (R_{ph}) parameter which represents the photodetecting performance and the ability of light absorbation quality of the photodiode. R_{ph} is defined as the ratio of the net photocurrent (I_{ph}) to the power of incoming light that effectively illuminating the photodiode and can be calculated by $R_{ph}=I_{ph}/P.A_{eff}$ formula [22], where I_{ph} is the net photocurrent ($I_{ph} = I_{light} - I_{dark}$), *P* is the incident light power intensity, and A_{eff} is the effectively illuminated area (6 mm^2) of the photodiode. For at -5 V of reverse bias, the R_{ph} responsivity values of the novel photodiode were calculated as 0.609 A/W (or 609 mA/W) and 0.398 A/W (or 398 mA/W) for the conditions of 20 mW/cm^2 and 100 mW/cm^2 of light power intensities, respectively. These huge responsivity values (as compared with the commercial ~0.5 A/W values) are found some similar to and some higher than some recently reported values [6,8,10,44].

Another important photodiode parameter is the photosensitivity (%PS) defined as a measure of a photodetector's capability of absorbing incident light. A high photosensitivity means a good light absorbtion. The unitless value of the %PS parameter can be found by a formula [22] given as $\%PS = [(I_{ph} - I_d)\times100]/I_d$, where I_d is dark current. For at 0 V, the %PS values of the CuAlFeMn/n-Si/Al photodiode were determined as 41.18 and 171.34 under 20 mW/cm^2 and 100 mW/cm^2 of light conditions, respectively. These values were found lower than some recently reported ones [10,45,46] due to the aforementioned high dark leakage current occurrence, similarly the %PS value of the device can be increased much more by suppressing the dark current, too.

Specific detectivity (*D**) of a photodiode is another figure of merit defined as a photodiode's ability to detect weak light signals. High detectivity photodiodes are utilized in optoelectronic communication applications. At shot-noise limit, dedectivity *D** normalized by the diode area (A_{eff}) can be found by using $D^*=R_{ph}/(2qI_d/A_{eff})^{1/2}$ formula [22], where *q* is electron charge. At reverse -5 V, the *D** value of the new photodiode was found as high as 2.21×10^{10} Jones and 7.07×10^9 for under 20 mW/cm^2 and 100 mW/cm^2 of light power intensities, respectively [10,45–47].

A photovoltaic photodiode or photodetector depends on separation of photo-excited electron-hole pairs. To see the photo-generated charge carriers as a sum of photocurrent in the produced photodiode the dynamic time-dependent (I-t) current-time (TPC test) curves obtained under different light conditions are given in Figure 5. According to these curves, a photovoltaic photocurrent generation proportional to the applied light power is occurs whenever the solar simulator's light is turned on. As the light is turned off, the current fells down to the ground dark level rapidly. As understood from this result, the produced photodiode exhibites good photovoltaic response behavior to the incident light.

The capacitance-voltage (C-V) measurements taken at varied step-increased frequencies between 10 kHz and 1 Mhz are presented in Figure 6. As seen on these C-V curves, in the reverse voltage bias region on the left side, there is an

increasing capacitance by decreasing frequency. The reason for that is explained as that the electrons cannot follow the ac current signal at these high frequencies [22]. On the right side at forward bias, there is seen an occurrence of negative capacitance which is also increasing by the decreasing frequency. Negative capacitance occurs when there is a change in charge that causes the net voltage falling on a material to change in the opposite direction such that a decrease in voltage results in an increase in charge [48–50].

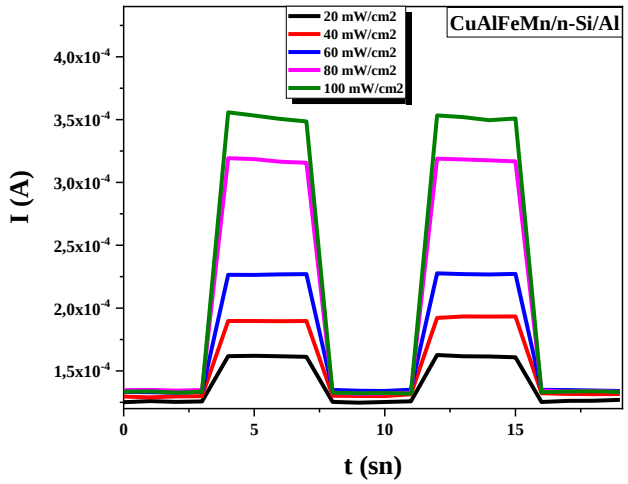

Fig.5. The time-dependent (*I-t*) TPC curves of the CuAlFeMn/n-Si/Al photodiode.

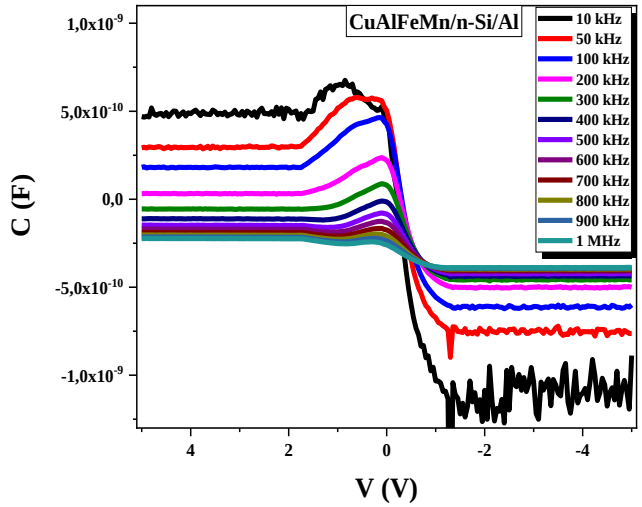

Fig.6. The capacitance-voltage curves of the novel CuAlMnNi/n-Si/Al photodiode obtained at different frequencies.

By drawing the inverse squared capacitance-voltage (C^{-2}-V) curves (presented in Figure 7) some of the electrical diode parameters of the produced photodiode were determined by this method, too. In the reverse biased region (on the left side of these curves) for the curve at 1 MHz the values of the non-compensated ionized donor atoms concentration (N_D) and diffusion potential (V_d) can be found by finding the the slope and linear extrapolation of the C^{-2}-V curve to the x-axis, respectively. The N_D can be calculated by the formula [22].given as below;

$$N_D = \frac{2}{q\varepsilon_0\varepsilon_S A^2}\left[\frac{d(C^{-2})}{dV}\right]^{-1} \quad (6)$$

where, C is capacitance of depletion layer, q is electron charge, A is diode area, ε_0 is permittivity of space, V is applied potential, ε_s is permittivity of the semiconductor and equal to 11.8 for n-Si. By substituting the slope value instead of the right $[d(C^{-2})/d(V)]^{-1}$ term in Eq.6, the N_d value was calculated as 1.54×10^{16} cm^{-3}. And by extrapolating the C^{-2}-V plot to the x-axis the V_d value was determined as 1.153 V. Apart from the I-V method, the Schottky barrier height (SBH) parameter ϕ_b can be also computed from the C^{-2}-V method by using the formula [22] given as below;

$$\phi_b = \frac{V_d}{n} + \frac{kT}{q} ln\left(\frac{N_C}{N_D}\right) \quad (7)$$

where; N_C is the effective density of states in the conduction band of n-Si ($N_C = 2.8 \times 10^{19}$ cm^{-3}). The ϕ_b value was found as 0.272 eV and this value was found lower than that value of 0.491 eV found by I-V method above for the dark condition. The effective Fermi energy (E_F) parameter was computed as 0.194 eV by using $E_F = \phi_b - (V_d/n)$ formula, too.

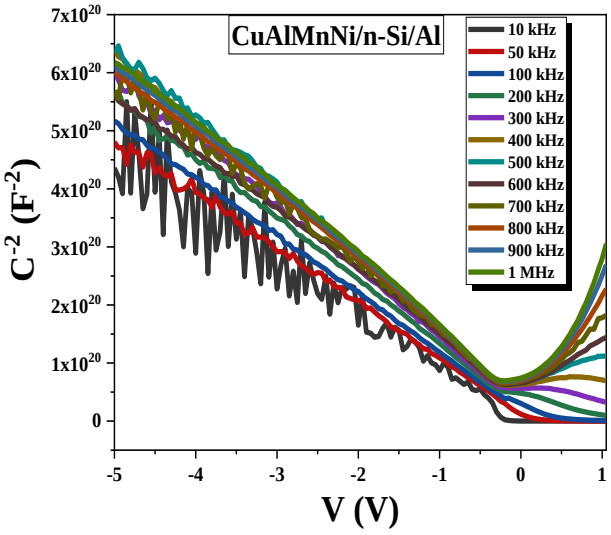

Fig.7. The inverse-squared C^{-2}-V curves of the new CuAlFeMn/n-Si/Al photodiode at different frequencies.

4. Conclusions

In this study, the new thin CuAlFeMn shape memory alloy film layered CuAlFeMn/n-Si/Al Schottky photodiode was successfully fabricated via using thermal evaporation method. The photo-electrical I-V, I-t and C-V characterization tests were performed on the new photodiode and some characteristic photo/electrical diode/photodiode parameters were determined. The high ideality factor of the device found deviated from unity was originated mainly from the existed interface states, vacancies, impurities, non-

uniform distribution of the interface charges and barrier non-homogeneity across the MS contact. The produced photodiode showed good photovoltaic and photoconductive properties. A huge high responsivity of 609 mA/W, photosensitivity (%PS) and a very well specific detectivity value of 2.21×10^{10} Jones were determined. The photosensitivity parameter of the photodevice found low can be improved by optimization of the interface quality. Negative capacitance was observed to occur on C-V tests. All obtained results implied that this novel thin film shape memory alloy layered CuAlFeMn/n-Si/Al photodiode can have potential usage in photodiode and photodetector dependent photovoltaic and optoelectronic applications.

Acknowledgements

This research work is a part of Ph.D. thesis works of Oktay KARADUMAN supervised by Prof. Dr. Canan Aksu CANBAY at Firat University, Faculty of Science, Department of Physics and was financially supported by FÜBAP, Project No: FF.21.14.

References

[1] S.M. Sze, K.N. Kwok, Physics of Semiconductor Devices, 3rd ed., John Wiley Sons Inc., Hoboken, New Jersey, 2006.

[2] F. Yakuphanoglu, Photovoltaic properties of the organic–inorganic photodiode based on polymer and fullerene blend for optical sensors, Sensors and Actuators A: Physical. 141 (2008) 383–389. https://doi.org/10.1016/j.sna.2007.10.023.

[3] A.A. Turturici, L. Abbene, G. Gerardi, F. Principato, Electrical characterization of CdTe pixel detectors with Al Schottky anode, Nuclear Instruments and Methods in Physics Research, Section A: Accelerators, Spectrometers, Detectors and Associated Equipment. 763 (2014) 476–482. https://doi.org/10.1016/j.nima.2014.07.011.

[4] H. Selvi, N. Unsuree, E. Whittaker, M.P. Halsall, E.W. Hill, A. Thomas, P. Parkinson, T.J. Echtermeyer, Towards substrate engineering of graphene-silicon Schottky diode photodetectors, Nanoscale. 10 (2018) 3399–3409. https://doi.org/10.1039/c7nr09591k.

[5] A. Tataroğlu, F.Z. Pür, The Richardson constant and barrier inhomogeneity at Au/Si 3N4/n-Si (MIS) Schottky diodes, Physica Scripta. 88 (2013). https://doi.org/10.1088/0031-8949/88/01/015801.

[6] A.G. Imer, E. Kaya, A. Dere, A.G. Al-Sehemi, A.A. Al-Ghamdi, A. Karabulut, F. Yakuphanoglu, Illumination impact on the electrical characteristics of Au/Sunset Yellow/n-Si/Au hybrid Schottky diode, Journal of Materials Science: Materials in Electronics. 31 (2020) 14665–14673. https://doi.org/10.1007/s10854-020-04029-8.

[7] S. Halder, B. Pal, A. Dey, S. Sil, P. Das, A. Biswas, P.P. Ray, Effect of graphene on improved photosensitivity of MoS2-graphene composite based Schottky diode, Materials Research Bulletin. 118 (2019). https://doi.org/10.1016/j.materresbull.2019.110507.

[8] S. Riazimehr, S. Kataria, J.M. Gonzalez-Medina, S. Wagner, M. Shaygan, S. Suckow, F.G. Ruiz, O. Engström, A. Godoy, M.C. Lemme, High Responsivity and Quantum Efficiency of Graphene/Silicon Photodiodes Achieved by Interdigitating Schottky and Gated Regions, ACS Photonics. 6 (2019) 107–115. https://doi.org/10.1021/acsphotonics.8b00951.

[9] D.H. Vieira, M. da Silva Ozório, G.L. Nogueira, L. Fugikawa-Santos, N. Alves, UV-photocurrent response of zinc oxide based devices: Application to ZnO/PEDOT:PSS hydrid Schottky diodes, Materials Science in Semiconductor Processing. 121 (2021). https://doi.org/10.1016/j.mssp.2020.105339.

[10] V. Balasubramani, J. Chandrasekaran, T.D. Nguyen, S. Maruthamuthu, R. Marnadu, P. Vivek, S. Sugarthi, Colossal photosensitive boost in Schottky diode behaviour with Ce-V2O5 interfaced layer of MIS structure, Sensors and Actuators, A: Physical. 315 (2020). https://doi.org/10.1016/j.sna.2020.112333.

[11] N. Camaioni, G. Casalbore-Miceli, G. Beggiato, M. Cristani, C. Summonte, Photoelectrical characterization of Schottky junctions between poly(4h-cyclopenta[2,1±b:3,4±b H]dithiophene) and aluminium: effect of hexadecyl groups in 4 position, Thin Solid Films. 366 (2000) 211–215. https://doi.org/doi.org/10.1016/S0040-6090(99)01103-7.

[12] R.H. Dyck, G.P. Weckler, Integrated Arrays of Silicon Photodetectors for Image Sensing, IEEE Transactions on Electron Devices. ED-15 (1968) 196–201. https://doi.org/10.1109/T-ED.1968.16166.

[13] M. Fontana, T. Deppe, A.K. Boyd, M. Rinzan, A.Y. Liu, M. Paranjape, P. Barbara, Electron-hole transport and photovoltaic effect in gated MoS2 Schottky junctions, Scientific Reports. 3 (2013) 1634. https://doi.org/10.1038/srep01634.

[14] Y.K. Lee, H. Lee, J.Y. Park, Tandem-structured, hot electron based photovoltaic cell with double Schottky barriers, Scientific Reports. 4 (2014). https://doi.org/10.1038/srep04580.

[15] M. Bendahan, J.L. Seguin, D. Lollman, H. Carchano, New type of Schottky barriers using NiTi shape memory alloy films, Thin Solid Films. 294 (1997) 278–280. https://doi.org/10.1016/S0040-6090(96)09230-9.

[16] J.A. Walker, K.J. Gabriel, M. Mehregany, Thin-film processing of TiNi shape memory alloy, Sensors and Actuators A: Physical. 21 (1990). https://doi.org/10.1016/0924-4247(90)85047-8.

[17] A. Isalgue, V. Torra, J.-L. Seguin, M. Bendahan, J.M. Amigo, V. Esteve-Cano, Shape memory NiTi thin films deposited at low temperature, Materials Science and Engineering A. 273–275 (1999) 717–721. https://doi.org/10.1016/S0921-5093(99)00403-7.

[18] C.A. Canbay, A. Tataroglu, A. Dere, A. Al-Ghamdi, F. Yakuphanoglu, A new shape memory alloy film/p-Si solar light four quadrant detector for solar tracking applications, Journal of Alloys and Compounds. 688 (2016) 762–768. https://doi.org/10.1016/J.JALLCOM.2016.07.087.

[19] C. Aksu Canbay, A. Dere, K. Mensah-Darkwa, A. Al-Ghamdi, Z. Karagoz Genç, R.K. Gupta, F. Yakuphanoglu, New type of Schottky diode-based Cu–Al–Mn–Cr shape memory material films, Applied Physics A: Materials Science and Processing. 122 (2016). https://doi.org/10.1007/s00339-016-0208-3.

[20] C.A. Canbay, A. Tataroğlu, A. Dere, A.G. Al-Sehemi, A. Karabulut, A.A. Al-Ghamdi, F. Yakuphanoglu, Electrical, kinetic and photoelectrical properties of CuAlMnMg shape memory alloy/n-Si Schottky diode, Journal of Alloys and Compounds. 888 (2021) 161600. https://doi.org/10.1016/J.JALLCOM.2021.161600.

[21] E. Aldirmaz, M. Guler, E. Guler, A. Dere, A. Tataroğlu, A.G. Al-Sehemi, A.A. Al-Ghamdi, F. Yakuphanoglu, A shape memory alloy based on photodiode for optoelectronic applications, Journal of Alloys and Compounds. 743 (2018) 227–233. https://doi.org/10.1016/J.JALLCOM.2018.01.380.

[22] C.A. Canbay, O. Karaduman, The photo response properties of shape memory alloy thin film based photodiode, Journal of Molecular Structure. 1235 (2021). https://doi.org/10.1016/j.molstruc.2021.130263.

[23] C.A. Canbay, A. Tataroğlu, W.A. Farooq, A. Dere, A. Karabulut, M. Atif, A. Hanif, CuAlMnV shape memory alloy thin film based photosensitive diode, Materials Science in Semiconductor Processing. 107 (2020) 104858. https://doi.org/10.1016/J.MSSP.2019.104858.

[24] E. Aldırmaz, A. Tataroğlu, A. Dere, M. Güler, E. Güler, A. Karabulut, F. Yakuphanoglu, Cu-Al-Mn shape memory alloy based Schottky diode formed on Si, Physica B: Condensed Matter. 560 (2019) 261–266. https://doi.org/10.1016/j.physb.2018.12.024.

[25] K. Otsuka, C.M. Wayman, Shape memory materials, Cambridge University Press, 1999.

[26] D.J. Fernandes, R. v. Peres, A.M. Mendes, C.N. Elias, Understanding the Shape-Memory Alloys Used in Orthodontics, ISRN Dentistry. 2011 (2011) 1–6. https://doi.org/10.5402/2011/132408.

[27] A. Concilio, V. Antonucci, F. Auricchio, L. Lecce, E. (Eds.). Sacco, Shape Memory Alloy Engineering, 2nd ed., Elsevier, 2021. https://doi.org/10.1016/C2018-0-02430-5.

[28] A. Rao, A.R. Srinivasa, J.N. Reddy, Introduction to shape memory alloys, SpringerBriefs in Applied Sciences and Technology. (2015) 1–31. https://doi.org/10.1007/978-3-319-03188-0_1.

[29] R. Kainuma, Recent progress in shape memory alloys, Materials Transactions. 59 (2018) 327–331. https://doi.org/10.2320/matertrans.M2017340.

[30] P. Krulevitch, A.P. Lee, P.B. Ramsey, J.C. Trevino, J. Hamilton, M. Allen, Thin film shape memory alloy microactuators, 1996. https://doi.org/10.1109/84.546407.

[31] Y.Q. Fu, J.K. Luo, A.J. Flewitt, W.M. Huang, S. Zhang, H.J. Du, W.I. Milne, Thin film shape memory alloys and microactuators, Int. J. Computational Materials Science and Surface Engineering. 2 (2009) 208–226. https://doi.org/10.1504/IJCMSSE.2009.027483.

[32] Y. Motemani, P.J.S. Buenconsejo, A. Ludwig, Recent Developments in High-Temperature Shape Memory Thin Films, Shape Memory and Superelasticity. 1 (2015). https://doi.org/10.1007/s40830-015-0041-0.

[33] B.T. Lester, T. Baxevanis, Y. Chemisky, D.C. Lagoudas, Review and perspectives: shape memory alloy composite systems, Acta Mechanica. 226 (2015) 3907–3960. https://doi.org/10.1007/s00707-015-1433-0.

[34] K.K. Alaneme, E.A. Okotete, Reconciling viability and cost-effective shape memory alloy options – A review of copper and iron based shape memory metallic systems, Engineering Science and Technology, an International Journal. 19 (2016) 1582–1592. https://doi.org/10.1016/j.jestch.2016.05.010.

[35] V.A. Chernenko, V.A. L'vov, E. Cesari, J.M. Barandiaran, Fundamentals of magnetocaloric effect in magnetic shape memory alloys, in: 2019: pp. 1–45. https://doi.org/10.1016/bs.hmm.2019.03.001.

[36] Y.Q. Fu, J.K. Luo, W.M. Huang, A.J. Flewitt, W.I. Milne, Thin film shape memory alloys for optical sensing applications, Journal of Physics: Conference Series. 76 (2007). https://doi.org/10.1088/1742-6596/76/1/012032.

[37] J. Mohd Jani, M. Leary, A. Subic, M.A. Gibson, A review of shape memory alloy research, applications and opportunities, Materials and Design. 56 (2014) 1078–1113. https://doi.org/10.1016/j.matdes.2013.11.084.

[38] C.A. Canbay, O. Karaduman, İ. Özkul, N. Ünlü, Modifying Thermal and Structural Characteristics of CuAlFeMn Shape Memory Alloy and a Hypothetical Analysis to Optimize Surface-Diffusion Annealing Temperature, Journal of Materials Engineering and Performance. 29 (2020) 7993–8005. https://doi.org/10.1007/S11665-020-05241-7.

[39] S.A. Baiz, C.A. Canbay, I. Ozkul, The investigation of thermodynamic and structural parameters in Cu-Al-Fe-Mn SMAs, in: AIP Conference Proceedings, American Institute of Physics Inc., 2018. https://doi.org/10.1063/1.5078910.

[40] C.A. Canbay, O. Karaduman, İ. Özkul, Lagging temperature problem in DTA/DSC measurement on investigation of NiTi SMA, Journal of Materials Science: Materials in Electronics. 31 (2020). https://doi.org/10.1007/s10854-020-03881-y.

[41] C. Canbay, O., Karaduman, P.A. Ibrahim, I. Ozkul, Thermostructural shape memory effect observations of ductile Cu-Al-Mn smart alloy, Advances in Materials Research. 10 (2021) 45–56.

https://doi.org/https://doi.org/10.12989/amr.2021.10.1.045.

[42] O. Karaduman, C. Aksu Canbay, N. Ünlü, S. Özkul, Analysis of a newly composed Cu-Al-Mn SMA showing acute SME characteristics, in: AIP Conference Proceedings, American Institute of Physics Inc., 2019. https://doi.org/10.1063/1.5135437.

[43] C.A. Canbay, O. Karaduman, N. Ünlü, S.A. Baiz, İ. Özkul, Heat treatment and quenching media effects on the thermodynamical, thermoelastical and structural characteristics of a new Cu-based quaternary shape memory alloy, Composites Part B: Engineering. 174 (2019). https://doi.org/10.1016/j.compositesb.2019.106940.

[44] P. Vivek, J. Chandrasekaran, R. Marnadu, S. Maruthamuthu, Fabrication of Illumination-Dependent Cu/p-Si Schottky Barrier Diodes by Sandwiching MoO 3 Nanoplates as an Interfacial Layer via JNSP Technique, (n.d.). https://doi.org/10.1007/s11664-020-08137-3.

[45] V. Balasubramani, J. Chandrasekaran, V. Manikandan, T.K. Le, R. Marnadu, P. Vivek, Upgraded photosensitivity under the influence of Yb doped on V2O5 thin films as an interfacial layer in MIS type Schottky barrier diode as photodiode application, Journal of Solid State Chemistry. 301 (2021). https://doi.org/10.1016/j.jssc.2021.122289.

[46] C.A. Canbay, O. Karaduman, The photo response properties of shape memory alloy thin film based photodiode, Journal of Molecular Structure. 1235 (2021) 130263. https://doi.org/10.1016/j.molstruc.2021.130263.

[47] U.Y. Won, B.H. Lee, Y.R. Kim, W.T. Kang, I. Lee, J.E. Kim, Y.H. Lee, W.J. Yu, Efficient photovoltaic effect in graphene/h-BN/silicon heterostructure self-powered photodetector, Nano Research. 14 (2021) 1967–1972. https://doi.org/10.1007/s12274-020-2866-x.

[48] A.K. Yadav, K.X. Nguyen, Z. Hong, P. García-Fernández, P. Aguado-Puente, C.T. Nelson, S. Das, B. Prasad, D. Kwon, S. Cheema, A.I. Khan, C. Hu, J. Íñiguez, J. Junquera, L.Q. Chen, D.A. Muller, R. Ramesh, S. Salahuddin, Spatially resolved steady-state negative capacitance, Nature. 565 (2019) 468–471. https://doi.org/10.1038/s41586-018-0855-y.

[49] R. Joly, S. Girod, N. Adjeroud, P. Grysan, J. Polesel-maris, Evidence of negative capacitance and capacitance modulation by light and mechanical stimuli in pt/zno/pt schottky junctions, Sensors. 21 (2021). https://doi.org/10.3390/s21062253.

[50] Ç. Bilkan, A. Gümüş, Ş. Altindal, The source of negative capacitance and anomalous peak in the forward bias capacitance-voltage in Cr/p-si Schottky barrier diodes (SBDs), Materials Science in Semiconductor Processing. 39 (2015) 484–491. https://doi.org/10.1016/j.mssp.2015.05.044.